DMD Fast Forward. Published on January 9, 2013 as DOI: 10.1124/dmd.112.050294
DMD Fast Forward. Published on January 9, 2013 as doi:10.1124/dmd.112.050294
This article has not been copyedited and formatted. The final version may differ from this version.

Application of a physiologically-based pharmacokinetic model to assess propofol hepatic and renal glucuronidation in isolation; utility of in vitro and in vivo data

Katherine L. Gill, Michael Gertz, J. Brian Houston and Aleksandra Galetin

Centre for Applied Pharmacokinetic Research, School of Pharmacy and Pharmaceutical Sciences, University of Manchester, Manchester, UK (K. L. G., M. G., J.B. H. and A. G.)

Downloaded from dmd.aspetjournals.org at ASPET Journals on April 18, 2024

Copyright 2013 by the American Society for Pharmacology and Experimental Therapeutics.

DMD Fast Forward. Published on January 9, 2013 as DOI: 10.1124/dmd.112.050294
This article has not been copyedited and formatted. The final version may differ from this version.

Running title: Applying a PBPK model to predict renal metabolism

Corresponding author: Dr A. Galetin

School of Pharmacy and Pharmaceutical Sciences,

University of Manchester, Stopford Building

Oxford Road,

Manchester, M13 9PT, UK

Tel: (+) 44 161 275 6886

Fax: (+) 44 161 275 8349

Email: Aleksandra.Galetin@manchester.ac.uk

Pages:	37
Tables:	4
Figures:	4
References:	68
Abstract:	243
Introduction	669
Discussion	1598

Abbreviations used are: ABT **=** 1-aminobenzotriazole; BSA = bovine serum albumin; CL_{int} = unbound intrinsic clearance; $CL_{int,CYP}$ = unbound intrinsic clearance by cytochrome P450; $CL_{int,UGT}$ = unbound intrinsic clearance by glucuronidation; CL_{IV} = intravenous clearance ; CYP = cytochrome P450; E_H = hepatic extraction ratio; E_R = renal extraction ratio; $f_{m,UGT}$ = fraction of metabolism due to glucuronidation; $f_{u,inc}$ = fraction unbound from protein in the incubation; HIM = human intestinal microsomes; HKM = human kidney microsomes; HLM = human liver microsomes; IVIVE = in vitro-in vivo extrapolation; K_p = tissue to blood concentration ratio; LC-MS/MS = liquid chromatography with tandem mass spectrometry; PBPK = physiologically-based pharmacokinetic; UDPGA = uridine diphosphate glucuronic acid; UGT = uridine diphosphate glucuronosyltransferase; V_{ss} = volume of distribution at steady state

Downloaded from dmd.aspetjournals.org at ASPET Journals on April 18, 2024

DMD Fast Forward. Published on January 9, 2013 as DOI: 10.1124/dmd.112.050294
This article has not been copyedited and formatted. The final version may differ from this version.

Abstract

A physiologically-based pharmacokinetic (PBPK) modeling approach was used to assess the prediction accuracy of propofol hepatic and extrahepatic metabolic clearance and address previously reported under-prediction of in vivo clearance based on static in vitro-in vivo extrapolation methods. The predictive capacity of propofol intrinsic clearance data (CL_{int}) obtained in human hepatocytes, liver and kidney microsomes was assessed using the PBPK model developed in Matlab. Microsomal data obtained by both substrate depletion and metabolite formation methods and in the presence of 2% BSA were considered in the analysis. Incorporation of hepatic and renal in vitro glucuronidation clearance in the PBPK model resulted in under-prediction of propofol clearance regardless of the source of in vitro data, as the predicted value did not exceed 35% of the observed clearance. Subsequently, propofol clinical data from three dose levels in intact patients and anhepatic subjects were used for the optimization of hepatic and renal CL_{int} in a simultaneous fitting routine. Optimization process highlighted that renal glucuronidation clearance was under-predicted to a greater extent than liver clearance, requiring empirical scaling factors of 17 and 9, respectively. The use of optimized clearance parameters predicted hepatic and renal extraction ratios within 20% of the observed values, reported in an additional independent clinical study. This study highlights the complexity involved in assessing the contribution of extrahepatic clearance mechanisms and illustrates the application of PBPK modelling, in conjunction with clinical data, to assess prediction of clearance from in vitro data for each tissue individually.

Downloaded from dmd.aspetjournals.org at ASPET Journals on April 18, 2024

DMD Fast Forward. Published on January 9, 2013 as DOI: 10.1124/dmd.112.050294
This article has not been copyedited and formatted. The final version may differ from this version.

Introduction

Propofol is a probe substrate for UGT1A9 and is also cleared by cytochrome P450 (CYP) enzymes, primarily via CYP2B6 and to a minor extent by CYP2C9, CYP1A2 and CYP3A4 (Guitton et al., 1998; Court et al., 2001; Oda et al., 2001; Court, 2005). Propofol has not been reported to be a substrate for transporters and undergoes minimal renal excretion (Vree et al., 1987; Simons et al., 1988; Veroli et al., 1992) and therefore, represents a good candidate for exploring the prediction of clearance due to metabolism alone. However, pronounced under-prediction of in vivo clearance has been observed for propofol using static in vitro-in vivo extrapolation (IVIVE) techniques (Kilford et al., 2009; Gill et al., 2012). Use of inappropriate in vitro systems, exclusion of extrahepatic metabolism, inadequacy of scaling factors and/or models applied to the in vitro data may all contribute to this under-prediction trend. Both in vivo and in vitro data indicate that the kidneys play an important role in the glucuronidation of certain drugs, including morphine and propofol (Mazoit et al., 1990; Pichette and du Souich, 1996; Soars et al., 2002; Takizawa et al., 2005a; Gill et al., 2012). Similarly, there is extensive evidence that both CYP and conjugation metabolism in the small intestine represent important contributors to drug clearance (Galetin et al., 2008; Cubitt et al., 2009; Gertz et al., 2010; Cubitt et al., 2011). Previously, we have shown that the inclusion of renal metabolic clearance data in IVIVE improved prediction of glucuronidation clearance; however, under-prediction was still apparent for certain drugs, including propofol (Gill et al., 2012).

Recently, there has been an increased use of dynamic modeling techniques such as physiologically-based pharmacokinetic (PBPK) models to predict drug exposure and clearance (Rowland et al., 2011; Huang and Rowland, 2012). The application of PBPK models by the pharmaceutical industry and regulatory bodies together with some of the limitations of this approach have been highlighted recently (Jones et al., 2011; Poulin et al., 2011; Zhao et al., 2011; Huang and Rowland, 2012). A variety of physiological and drug specific parameters, including in vitro and in vivo clearance and tissue binding data, can be incorporated to optimize these models and improve prediction of in vivo pharmacokinetics (Nestorov, 2007; Huang and Rowland, 2012). The relative accuracy of predictions of hepatic versus extrahepatic clearance from in vitro data has not previously been assessed as the availability of in vivo data to allow such analysis is very limited. However, the use of a dynamic approach such as PBPK modeling in conjunction with suitable in vivo data would be

Downloaded from dmd.aspetjournals.org at ASPET Journals on April 18, 2024

DMD Fast Forward. Published on January 9, 2013 as DOI: 10.1124/dmd.112.050294
This article has not been copyedited and formatted. The final version may differ from this version.

expected to improve the understanding of the predictive capacity of in vitro clearance data for different tissues in isolation.

Previous PBPK modeling for propofol has not incorporated in vitro hepatic clearance data and has ignored the contribution of renal metabolic clearance (Levitt and Schnider, 2005; Upton and Ludbrook, 2005). In vivo propofol concentration-time data for subjects during liver transplantation have been reported in the literature (Veroli et al., 1992); under these conditions the clearance observed is solely mediated by extrahepatic metabolism. Such in vivo data used in conjunction with mechanistic PBPK models allows independent assessment of the predictive capacity of in vitro clearance data for hepatic and renal metabolism.

The aim of this study was to apply a PBPK model to assess the prediction of propofol systemic clearance using in vitro metabolism data from the kidney and liver. Propofol blood concentration-time profiles and systemic clearance following intravenous dosing were predicted using intrinsic clearance (CL_{int}) data obtained in different in vitro systems (microsomes and hepatocytes); the predictive ability of hepatic in vitro CL_{int} data from different sources was assessed. The rich in vivo data available for propofol were used to optimize the PBPK model and bridge the gap in the IVIVE of propofol clearance. In vivo data from anhepatic patients allowed the analysis of the prediction success of renal glucuronidation clearance in isolation from the liver; in conjunction with data from intact patients these data were used to refine the prediction of renal and hepatic clearance.

Downloaded from dmd.aspetjournals.org at ASPET Journals on April 18, 2024

DMD Fast Forward. Published on January 9, 2013 as DOI: 10.1124/dmd.112.050294
This article has not been copyedited and formatted. The final version may differ from this version.

Materials and Methods

Chemicals. Propofol, alamethicin (from *Trichoderma viride*), UDP-glucuronic acid (UDPGA), EDTA, bovine serum albumin (BSA), saccharic acid lactone, $MgCL_2$, $NADP^+$, isocitric acid and isocitric acid dehydrogenase were purchased from Sigma-Aldrich® (Gillingham, Dorset, UK). Propofol glucuronide was purchased from Toronto Research Chemicals (North York, Ontario, Canada). All other reagents were of the highest grade available.

Source of the microsomes. BD UltraPool™ human liver microsomes (HLM) were purchased from BD Gentest (Woburn, MA). HLM were pooled from 150 Caucasian donors, with 50% female and a mean age of 53 years (range 18-79 years). Pooled human kidney and intestine microsomes (HKM and HIM) were purchased from XenoTech (Tebu-Bio Ltd., Peterborough, Cambridgeshire, UK). HKM were pooled from 8 donors; with 88% Caucasian, 50% female and a mean age of 61 years (range 48-69 years). HIM were pooled from 13 donors; with 92% Caucasian, 46% female and a mean age of 40 years (range 18-55 years). Microsomes were stored at -80°C. Activity for pooled HLM was reported as 0.054 nmol/min/mg protein for CYP2B6 and 2.00 nmol/min/mg protein for UGT1A9, using specific probe substrates. For HKM and HIM pools glucuronidation capacity was characterized for 4-methylumbelliferone (a substrate of multiple UGTs); with reported activity of 125 and 7.22 nmol/min/mg protein, respectively.

Experimental conditions for microsomal CYP depletion assays. Incubations were performed in duplicate in Eppendorf vials using a substrate depletion approach. A final substrate concentration of 3 µM was used, which is > 3-fold below the reported K_m (Michaelis-Menten constant) value in HLM (Guitton et al., 1998; Court et al., 2001; Al-Jahdari et al., 2006), ensuring suitable conditions to determine the intrinsic clearance of propofol. Propofol was preincubated at a microsomal protein concentration of 0.5 mg/ml in 0.1 M phosphate buffer, pH 7.4 for 5 min at 37°C shaken at 900 rpm using an Eppendorf thermomixer (Hamburg, Germany) (Kilford et al., 2009). The reaction was initiated by addition of the NADPH regenerating system, containing 1 mM $NADP^+$, 7.5 mM isocitric acid, 1 unit/ml isocitric acid dehydrogenase and 10 mM $MgCL_2$ in a final incubation volume of 1 ml (Kilford et al., 2009). Concentration of the organic solvent used (methanol) was 0.5% v/v of the incubation media. The total length of the incubation was 45 min. To terminate the reaction 100 µl samples of the incubation were removed at each time point and added to an equal volume of ice-cold methanol containing 1 µM tolbutamide as the internal standard. Samples were kept at -20°C for at

Downloaded from dmd.aspetjournals.org at ASPET Journals on April 18, 2024

DMD Fast Forward. Published on January 9, 2013 as DOI: 10.1124/dmd.112.050294
This article has not been copyedited and formatted. The final version may differ from this version.

least 1 h and then centrifuged (MSE Mistral 3000i centrifuge, London, UK) at 4°C and 2500 rpm for 30 min. An aliquot of the supernatant (30 µl) was analyzed by LC-MS/MS for propofol concentration. Experiments were repeated on three separate occasions. No CYP clearance was observed in HKM and HIM in the absence of BSA.

Experiments performed in the presence of BSA used the same methodology, with the exception of the addition of 2% BSA to the incubation. Samples of 100 µl of the incubation were removed at each time point and added to double volume of ice-cold acetonitrile containing 1 µM tolbutamide to terminate the reaction. Samples were refrigerated for at least 10 min and then centrifuged (Eppendorf Mini Spin, Hamburg, Germany) at 13400 rpm and room temperature for 5 min prior to analysis by LC-MS/MS for propofol concentration. Similarly to data in the absence of BSA, no CYP clearance was observed in HKM and HIM in the presence of BSA. Non-enzymatic depletion of propofol was monitored and clearance estimates were corrected for the observed non-enzymatic loss.

Experimental conditions for propofol glucuronide formation in microsomes. Incubations were performed in duplicate using Eppendorf vials. Initial experiments showed propofol glucuronide formation was linear up to 10 min at protein concentrations ≤ 0.5 mg/ml in all three tissues, both in the presence and absence of 2% BSA. The time period and protein concentration for each tissue were selected to ensure metabolite formation was within the linear range. Substrate concentrations ranging from 0.5 to 400 µM were used to assess the kinetic parameters K_m and V_{max} (maximum rate of reaction), with the exception of HIM where a concentration range of 2.5 to 600 µM was employed. Microsomal protein concentrations for experiments performed in the absence of BSA were 0.2, 0.1 and 0.4 mg/ml for HLM, HKM and HIM, respectively. Microsomes were treated with alamethicin (50 µg/mg protein) for 15 min on ice as reported previously (Fisher et al., 2000; Cubitt et al., 2009; Kilford et al., 2009). Activated microsomes were preincubated with propofol and 0.1 M phosphate buffer, pH 7.1, containing 3.45 mM $MgCL_2$, 1.15 mM EDTA and 115 µM saccharic acid lactone, for 5 min at 37°C shaken at 900 rpm (Fisher et al., 2001; Cubitt et al., 2009; Kilford et al., 2009). The reaction was initiated by the addition of UDPGA (5 mM in incubation), to give a final incubation volume of 0.1 ml. Organic solvent (methanol) made up 1% v/v of the incubation media. Control incubations were performed with no cofactor present to account for any potential cofactor independent formation of the metabolite over the incubation time. In the absence of BSA, the reaction was terminated after 10 mins by addition of an equal volume ice-cold methanol containing 1 µM of the

Downloaded from dmd.aspetjournals.org at ASPET Journals on April 18, 2024

DMD Fast Forward. Published on January 9, 2013 as DOI: 10.1124/dmd.112.050294
This article has not been copyedited and formatted. The final version may differ from this version.

internal standard tolbutamide. Samples with starting propofol concentrations in excess of 10 µM were diluted in ice cold blank 1:1 matrix : methanol to give a final propofol concentration of ≤ 10 µM. Samples were kept at -20°C for at least 1 h and then centrifuged (MSE Mistral 3000i centrifuge, London, UK) at 4°C and 2500 rpm for 30 min. An aliquot of the supernatant (20 µl) was analyzed by LC-MS/MS for propofol glucuronide concentration.

Incubation conditions for experiments including BSA were comparable to those without BSA, with the exception of the addition of 2% BSA. Optimal conditions of 0.1 mg/ml microsomal protein for HLM and HKM or 0.2 mg/ml for HIM were employed for the kinetic assessment in the presence of BSA. The reaction was terminated after 10 mins by addition of double volume ice-cold acetonitrile containing 1 µM of the internal standard tolbutamide. Samples with starting propofol concentrations in excess of 10 µM were diluted in ice cold blank 1:2 matrix : acetonitrile to give a final propofol concentration of ≤ 10 µM. Samples including BSA were refrigerated for at least 10 min and then centrifuged (Eppendorf Mini Spin, Hamburg, Germany) at 13400 rpm and room temperature for 5 min. An aliquot of the supernatant (20 µl) was analyzed by LC-MS/MS for propofol glucuronide concentration. Experiments were repeated on three separate occasions.

Propofol intrinsic clearance due to glucuronidation ($CL_{int,UGT}$) data in HLM, HKM and HIM obtained by the depletion method and corresponding incubation details have been reported previously (Gill et al., 2012). The batch of HLM and HKM used were the same as those used herein for determination of intrinsic clearance due to CYPs ($CL_{int,CYP}$) and metabolite formation $CL_{int,UGT}$. A different pool of HIM was used due to the limited supply of the batch used previously; the donor demographics and activity characterization were comparable between the two HIM pools.

In addition to microsomal data, use of in house unbound CL_{int} data obtained in hepatocytes at a single propofol concentration of 5 µM was also investigated. CL_{int} data were generated by the substrate depletion approach using pooled cryopreserved human hepatocytes from 10 donors purchased from In Vitro Technologies (Baltimore, USA). Experiments were performed in the absence and presence of nonspecific CYP inhibitor 1-aminobenzotriazole (ABT) at 2.5 mM to determine total CL_{int} (combined $CL_{int,CYP}$ and $CL_{int,UGT}$) and $CL_{int,UGT}$, respectively.

LC-MS/MS. Propofol and propofol glucuronide were analyzed on a Waters 2790 or an Agilent 1100 HPLC system, respectively, with a Micromass Quattro Ultima triple quadruple mass spectrometer in negative mode. Source temperature was 125°C, desolvation temperature was 350°C,

Downloaded from dmd.aspetjournals.org at ASPET Journals on April 18, 2024

DMD Fast Forward. Published on January 9, 2013 as DOI: 10.1124/dmd.112.050294
This article has not been copyedited and formatted. The final version may differ from this version.

desolvation gas flow rate was 600 l/h. Cone gas flow rate was 150 l/h for propofol and 50 l/h for propofol glucuronide. The capillary voltage was 3.25 kV. Propofol and propofol glucuronide were analyzed using single ion recording due to their limited fragmentation. The transitions for propofol, propofol glucuronide and tolbutamide were 176.90, 353.55 and 269.00 m/z, respectively. Analytes were separated using a Luna C18 (3 µ, 50 x 4.6 mm) column (Phenomenex, Macclesfield, UK). Four mobile phases were used, with varying gradients for each compound; A) 90% water, 10% methanol and 0.05% formic acid; B) 10% water, 90% methanol and 0.05% formic acid; C) 90% water, 10% methanol and 1 mM ammonium acetate; D) 10% water, 90% methanol and 1 mM ammonium acetate. The flow rate was 1 ml/min, splitting to 0.25 ml/min prior to entry into the mass spectrometer. Cone voltage was set to 60 V for propofol and 75 V for tolbutamide, and the corresponding retention times were 3.40 and 2.80 min. When analyzing for the metabolite the cone voltage was set to 30 and 45 V for propofol glucuronide and tolbutamide, with retention times of 3.40 and 3.20 min, respectively. The lower limit of quantification for propofol and its glucuronide metabolite were 0.039 and 0.020 µM.

Data analysis. The mean propofol concentrations of the duplicate samples from the CYP depletion assays at each timepoint were analyzed using GraFit 5 (Erithacus Software, Horley, UK) to determine the elimination rate constant (k) by fitting a single exponential equation to the data. This rate constant was used to calculate the $CL_{int,CYP}$ (Equation 1). The non-enzymatic loss was taken into account when analyzing the experimental data. The $CL_{int,CYP}$ values were corrected for nonspecific binding ($CL_{int,CYP}/f_{u,inc}$), using the experimentally determined fraction unbound in the microsomal incubation ($f_{u,inc}$) in the presence and absence of 2% BSA reported previously (Gill et al., 2012), to generate the unbound intrinsic clearance (µl/min/mg protein). The unbound $CL_{int,CYP}$ values have been reported.

$$CL_{int,CYP} = \frac{k \times \text{volume of incubation}}{\text{amount of microsomal protein in assay}} \quad (1)$$

The mean propofol glucuronide formation rates of the duplicate samples across the employed propofol concentration range were analyzed using nonlinear regression in GraFit 5. K_m and V_{max} were determined by fitting the Michaelis-Menten equation to the data. Binding of propofol to microsomal protein and albumin has been shown to be independent of substrate concentration over the range of propofol concentrations used herein (Rowland et al., 2008; Rowland et al., 2009). The K_m values were corrected for nonspecific binding in the presence and absence of 2% BSA, using data reported

Downloaded from dmd.aspetjournals.org at ASPET Journals on April 18, 2024

DMD Fast Forward. Published on January 9, 2013 as DOI: 10.1124/dmd.112.050294
This article has not been copyedited and formatted. The final version may differ from this version.

previously (Gill et al., 2012), to give unbound K_m. The ratio of V_{max} and unbound K_m values were used to calculate the $CL_{int,UGT}$. Unbound $CL_{int,UGT}$ and K_m values have been reported.

In vitro CL_{int} data obtained using HLM in the presence of either CYP or UGT cofactors were used to determine the fraction of metabolism due to glucuronidation ($f_{m,UGT}$) (Equation 2) (Kilford et al., 2009). Similarly, CL_{int} data derived in hepatocytes in the presence or absence of ABT were used to determine the $f_{m,UGT}$.

$$f_{m,UGT} = \frac{CL_{int,UGT}}{CL_{int,UGT}+CL_{int,CYP}} \quad (2)$$

In vitro microsomal CL_{int} data from the various assays were scaled with the microsomal protein yields; 40, 12.8 and 20.6 mg of protein/g tissue were used for hepatic, renal and intestinal data, respectively (Al-Jahdari et al., 2006; Barter et al., 2007; Cubitt et al., 2009). Hepatocyte unbound CL_{int} data were scaled with a hepatocellularity value of 120 x 10^6 cells/g tissue (Brown et al., 2007). The scaled CL_{int} data were compared between the in vitro systems.

Development of the propofol PBPK model. A previously reported in house whole body PBPK model (Gertz et al., 2011) was adapted to predict propofol concentration-time profiles and pharmacokinetics. The resultant model contained 14 organ compartments connected by arterial and venous blood supplies (Figure 1). An additional compartment representing the rest of the body was included which accounted for < 5% of the total body weight and < 8% the total blood flow. Propofol plasma binding, blood to plasma partition coefficient and renal excretion of unchanged drug were collated from the literature, as reported previously (Gill et al., 2012). Tissue to plasma concentration ratios (K_p) were predicted using the Rodgers and Rowland method (Rodgers and Rowland, 2006), and are detailed in Figure 1 and Supplemental Data Table 1. Tissue blood flow and volume were collated from the literature (ICRP, 2002) (Figure 1 and Supplemental Data Table 1).

All tissues were assumed to be well stirred compartments where unbound tissue concentration is at equilibrium with the unbound concentration in the emerging blood (Pang and Rowland, 1977). Equation 3 was used for non-eliminating organs (Nestorov, 2003).

$$\frac{dC_T}{dt} = Q_T\left(C_{b,A} - \frac{C_T}{K_{b,T}}\right)/V_T \quad (3)$$

where C_T, Q_T, $C_{b,A}$, $K_{b,T}$ and V_T represent unbound tissue concentration, tissue blood flow, unbound concentration in arterial blood, tissue to blood concentration ratio and tissue volume.

The liver, kidney and enterocytes were considered to potentially contribute to systemic drug clearance. The liver and kidney were separated into cellular tissue and blood compartments to allow

Downloaded from dmd.aspetjournals.org at ASPET Journals on April 18, 2024

DMD Fast Forward. Published on January 9, 2013 as DOI: 10.1124/dmd.112.050294
This article has not been copyedited and formatted. The final version may differ from this version.

assessment of the extraction ratio across each tissue. Equation 4 represents the tissue compartment and Equation 5 represents the blood compartment for the kidney and the liver.

$$\frac{dC_{T,c}}{dt} = \left[PS_T\left(f_{u,b} \cdot C_{T,b} - \frac{f_{u,b}}{K_{b,T}} \cdot C_{T,c}\right) - \frac{f_{u,b}}{K_{b,T}} \cdot C_{T,c} \cdot \left(CL_{int,UGT} + CL_{int,CYP}\right)\right] / V_{T,c} \quad (4)$$

$$\frac{dC_{T,b}}{dt} = \left(Q_T \cdot C_{b,A} - Q_T \cdot C_{T,b} - PS_T\left(f_{u,b} \cdot C_{T,b} - \frac{f_{u,b}}{K_{b,T}} \cdot C_{T,c}\right)\right) / V_{T,b} \quad (5)$$

where $C_{T,c}$, PS_T, $C_{T,b}$, $f_{u,b}$, $V_{T,c}$, and $V_{T,b}$ represent tissue cell concentration, permeability surface area (set to > 10,000 x tissue blood flow to ensure perfusion limited kinetics), concentration in blood residing in the tissue, blood binding, volume of tissue cells and volume of blood residing in tissue. Microsomal $CL_{int,UGT}$ and $CL_{int,CYP}$ were scaled with the microsomal recovery and mass of the relevant tissue, as detailed above. Hepatocyte CL_{int} (combined $CL_{int,UGT}$ and $CL_{int,CYP}$) data were scaled with the hepatocellularity value and the mass of the liver. Kidney and liver blood volumes were set to 100 ml (ICRP, 2002). The portal vein concentration represents the differential of emergent blood concentrations from the large and small intestine, enterocytes, stomach, spleen and pancreas.

The extraction ratio for the enterocytes was not calculated and therefore this tissue was defined as a single compartment (Equation 6).

$$\frac{dC_T}{dt} = \left[Q_T\left(C_{b,A} - \frac{C_T}{K_{b,T}}\right) - \frac{f_{u,b}}{K_{b,T}} \cdot C_T \cdot \left(CL_{int,UGT} + CL_{int,CYP}\right)\right] / V_T \quad (6)$$

The blood flow to the small intestine represents approximately 10% of the cardiac output (ICRP, 2002) and the enterocytic blood flow represents approximately 50% of the small intestinal blood flow (Gertz et al., 2011). The rate equations were solved in Matlab v 7.12.0® (2011a) using the ODE15s solver. The dose recovery over time was assessed using mass balance equations.

Assumptions applied to the propofol PBPK model. The following assumptions were made: 1. there is no active uptake or efflux of propofol in any tissue and therefore tissue distribution/elimination is perfusion rate limited; this assumption seems justifiable as together with the high lipophilicity of propofol (Reiner et al., 2009) there is a lack of in vitro or in vivo data suggesting that propofol is a substrate of transporters; 2. propofol does not affect the cardiac output (Grounds et al., 1985; Price et al., 1992); 3. the volume of distribution at steady state (V_{ss}) for the anhepatic patients was not expected to be markedly different from that in healthy subjects. This is supported by a number of studies where changes in V_{ss} for patients with varying grades of liver cirrhosis were not apparent in comparison to patients with healthy livers (mean values ranging from 202 to 637 l in subjects with mild liver cirrhosis) (Servin et al., 1988a; Servin et al., 1988b; Servin et al., 1990).

Downloaded from dmd.aspetjournals.org at ASPET Journals on April 18, 2024

DMD Fast Forward. Published on January 9, 2013 as DOI: 10.1124/dmd.112.050294
This article has not been copyedited and formatted. The final version may differ from this version.

Similarly, no changes in propofol V_{ss} during chronic hepatic cirrhosis were stated in Propofol Product Monograph (www.astrazeneca.ca/documents/ProductPortfolio/DIPRIVAN_PM_en.pdf). In addition, no change in blood binding of propofol was observed in patients with mild liver cirrhosis (Servin et al., 1990).

Validation of propofol PBPK model. The PBPK model was validated using data from two clinical studies, covering a propofol dose range of 2 – 18 mg/kg propofol (Gepts et al., 1987; Doenicke et al., 1997). The study details and subject demographics for these studies are presented in Table 1. The cardiac output was corrected for the mean age of each dose group (Brown et al., 1997). One of the studies (Gepts et al., 1987), included elderly subjects but no alterations were made to the tissue volumes for this population. Plasma binding was assumed to be equivalent in young and elderly subjects for which evidence could be found in the literature (Kirkpatrick et al., 1988). Minimal age and gender effects have been observed for in vitro microsomal UGT activity for a range of probe substrates including propofol (Court, 2010); therefore, no alterations were made to microsomal protein yields for the different populations.

V_{ss} for propofol is highly variable in the literature (mean values reported in 14 studies collated from the literature (including 194 subjects) range from 121 to 722 l); no trends were observed regarding gender, age, dose level, length of infusion or disease status (details provided in Supplemental Data; Figure 1). The V_{ss} data considered for this analysis were taken from studies where the propofol blood concentrations were available over at least 8 hours which is considered adequate to describe its pharmacokinetics. Where necessary the predicted K_p values were optimized using a universal scalar for all tissues to ensure that the reported V_{ss} was recovered correctly for each dose group used in the model validation and for the prediction of propofol blood concentration-time profiles.

Contradicting reports exist in the literature over the potential propofol metabolism and/or sequestration in the lung (Dawidowicz et al., 2000; He et al., 2000; Hiraoka et al., 2005; Takizawa et al., 2005a). Reduction in propofol concentration across the lung in one of the studies was proportional to the formation of the quinol metabolite and assessment of the blood concentration data suggested a lung extraction ratio of 0.40 (Dawidowicz et al., 2000). Assumption of that extent of lung extraction would predict clearance in excess of the observed values for the in vivo studies used in the current analysis. In contrast, the majority of other available data proposed that the reduction in propofol

Downloaded from dmd.aspetjournals.org at ASPET Journals on April 18, 2024

DMD Fast Forward. Published on January 9, 2013 as DOI: 10.1124/dmd.112.050294
This article has not been copyedited and formatted. The final version may differ from this version.

concentration across the lung was not due to metabolism but binding, with subsequent slow release from the lung (He et al., 2000; Hiraoka et al., 2005; Levitt and Schnider, 2005; Takizawa et al., 2005a; Upton and Ludbrook, 2005). Previous studies showed that sequestration of propofol was not apparent following intravenous infusion dosing, particularly for patients of > 35 years (He et al., 2000; Levitt and Schnider, 2005). The majority of the in vivo data used in the current analysis were reported in subjects of similar or greater age following an infusion dose, which may explain the lack of evidence for sequestration in the lung. With the lack of suitable data to define association and dissociation rate constants for potential propofol binding in the lung, a truly physiological model to account for this process could not have been included within the current PBPK model and therefore no adjustment for lung sequestration was employed. Accumulation within lysosomes, one potential route of sequestration within tissues such as lungs, is not anticipated for propofol due to its physicochemical properties. The potential for propofol sequestration in other tissues or via other mechanisms could not be investigated, although this cannot be ruled out.

In vitro clearance data used as inputs for the PBPK model to predict in vivo clearance of propofol. In vitro $CL_{int,CYP}$ and $CL_{int,UGT}$ data for HLM, HKM and HIM were used within the PBPK model to assess the success of in vivo clearance predictions. The prediction success of systemic clearance was investigated using $CL_{int,UGT}$ data from substrate depletion assays (obtained previously, (Gill et al., 2012)) and metabolite formation assays (current study). $CL_{int,CYP}$ data were obtained using the substrate depletion approach (detailed herein). Clearance prediction success for in house data determined via the substrate depletion method in hepatocytes (combined $CL_{int,CYP}$ and $CL_{int,UGT}$) in conjunction with $CL_{int,UGT}$ data from HKM and HIM from either the substrate depletion or metabolite formation methods was also investigated. Details of the in vitro data used for prediction of in vivo clearance are given in Table 2.

In addition, the in vitro data were used in the PBPK model to predict hepatic and renal extraction ratios (E_H and E_R, respectively) at steady state. The predicted extraction ratios were compared to values reported in a clinical study (Hiraoka et al., 2005), which was independent to the clinical studies used for model validation. The reported E_H (0.93) and E_R (0.69) were obtained from blood concentration measurements in the renal vein, hepatic vein and radial artery at steady state. The extraction ratios for each tissue (E_T) were calculated by Equation 7.

$$E_T = \frac{C_{b,in} - C_{T,b}}{C_{b,in}} \quad (7)$$

Downloaded from dmd.aspetjournals.org at ASPET Journals on April 18, 2024

DMD Fast Forward. Published on January 9, 2013 as DOI: 10.1124/dmd.112.050294
This article has not been copyedited and formatted. The final version may differ from this version.

Where $C_{b,in}$ represents the concentration in blood entering the tissue.

Optimization of predictions of renal and hepatic clearance from in vitro data. Initial analysis indicated under-prediction of hepatic and renal CL_{int}, regardless of the in vitro system used. Therefore, optimization was performed to bridge the gap in IVIVE and determine the empirical scaling factors required for the in vitro data to accurately recover in vivo clearance, by fitting the PBPK model to the in vivo propofol blood concentration-time profiles. Data from three dose levels (6 – 18 mg/kg) in intact patients (Gepts et al., 1987) and from anhepatic patients (Veroli et al., 1992) (who received a 0.5 mg/kg dose) were fitted simultaneously in Matlab using a nonlinear least squared regression analysis (lsqnonlin function). For the anhepatic patients the PBPK model was adapted removing the liver compartment to reflect the in vivo situation. Data from the anhepatic patients were used to delineate the contribution of the renal $CL_{int,UGT}$ and refine the PBPK model with respect to renal metabolism , whereas data from intact patients provided input for optimization of the hepatic CL_{int} and K_p. Propofol concentration-time profiles in the anhepatic patients were only available for 1 h and therefore V_{ss} for these patients could not be determined from the profile. The data from intact patients were used to inform the optimization of the V_{ss} for both intact and anhepatic patients in the simultaneous fitting routine. Optimization of hepatic and renal CL_{int} in the PBPK model allowed the assessment of the degree of under-prediction of in vitro CL_{int} for each tissue individually.

The in vitro CL_{int} data for the intestinal microsomes was low in comparison to that in the kidney and the liver. Considering their lower tissue mass and blood flow, the enterocytes were not expected to contribute extensively to the metabolism of propofol. There is also a lack of suitable in vivo data for assessment of the predictive capacity of the intestinal in vitro $CL_{int,UGT}$ data. For these reasons the optimization was performed for the kidney and liver metabolism only.

Downloaded from dmd.aspetjournals.org at ASPET Journals on April 18, 2024

DMD Fast Forward. Published on January 9, 2013 as DOI: 10.1124/dmd.112.050294
This article has not been copyedited and formatted. The final version may differ from this version.

Results

Propofol CYP depletion assays in human hepatic, renal and intestinal microsomes. No CYP mediated clearance was observed in renal or intestinal microsomes; however, in the liver, $CL_{int,CYP}$ in the presence of BSA was 2.2-fold higher than $CL_{int,UGT}$ obtained via substrate depletion (Table 2). BSA increased propofol $CL_{int,CYP}$ by 2-fold in HLM (Table 2), whereas a 3-fold change in $CL_{int,UGT}$ in the presence of BSA was reported previously (Gill et al., 2012). Depletion profiles in HLM over time are shown in the Supplemental Data, Figure 2.

Propofol glucuronide formation assays in human hepatic, renal and intestinal microsomes. Propofol K_m and V_{max} were determined in hepatic, renal and intestinal microsomes both in the presence and absence of BSA; corresponding kinetic profiles are shown in Figure 2. Use of a protein concentration of 0.1 mg/ml for HLM and HKM in combination with 2% BSA had no impact on propofol V_{max}. However, use of lower microsomal protein concentrations (0.05 and 0.075 mg/ml) in the presence of BSA reduced V_{max} by up to 70% (Supplemental Data, Figure 3 A and B). The extent of the decrease in V_{max} observed at the lowest protein concentration was more pronounced in the kidney than the liver (3-fold versus 2-fold). Use of a 1% BSA concentration produced comparable results to data obtained in the presence of 2% BSA (Supplemental Data, Figure 3 C and D).

In the absence of BSA propofol K_m was similar in HLM and HKM (107 versus 91 μM), however, the value for the intestine was greater (458 μM) (Table 2). Inclusion of 2% BSA caused reduction in K_m for all tissues, which was more pronounced in the liver and kidney than in the intestine, with K_m values of 5, 3 and 133 μM in the presence of BSA, respectively (Table 2). Similarly to data derived in the absence of BSA, K_m values in the presence of 2% BSA were comparable in HLM and HKM. Under optimal conditions inclusion of 2% BSA had no appreciable impact on V_{max} in any of the tissues (Table 2). Scaled $CL_{int,UGT}$ values (mL/min/g tissue) were highest in HKM both in the presence and absence of BSA (Table 2). Upon inclusion of 2% BSA, $CL_{int,UGT}$ in HIM increased by 4-fold in comparison to the large increases observed for HLM (18-fold) and HKM (23-fold) (Table 2).

Comparison of CL_{int} data derived using different in vitro systems. In the absence of BSA, propofol scaled $CL_{int,UGT}$ estimates derived from metabolite formation assays in HLM and HKM were lower than those from substrate depletion assays (0.6 versus 2.7 ml/min/g tissue and 0.7 versus 1.2 ml/min/g tissue, respectively) (Table 2). However, in the presence of 2% BSA, $CL_{int,UGT}$ data were comparable from both assays (Table 2). Consequently, the increase in propofol $CL_{int,UGT}$ upon

Downloaded from dmd.aspetjournals.org at ASPET Journals on April 18, 2024

DMD Fast Forward. Published on January 9, 2013 as DOI: 10.1124/dmd.112.050294
This article has not been copyedited and formatted. The final version may differ from this version.

inclusion of BSA in HLM and HKM was greater for the metabolite formation data in comparison with the substrate depletion data. For HIM, $CL_{int,UGT}$ estimates obtained by metabolite formation were lower both in the presence (9-fold) and absence (22-fold) of BSA compared to those obtained by depletion (Table 2). Combined $CL_{int,CYP}$ and $CL_{int,UGT}$ data for hepatic microsomes (26 and 29 ml/min/g tissue using the depletion or formation assays in the presence of BSA, respectively) gave higher total CL_{int} per gram of liver than estimates obtained from hepatocytes (18 ml/min/g tissue).

The in vitro $f_{m,UGT}$ for HLM CL_{int} data derived using substrate depletion were 0.23 and 0.31 in the absence and presence of 2% BSA, respectively. When using HLM $CL_{int,UGT}$ data derived via metabolite formation in the presence of BSA the resulting $f_{m,UGT}$ (0.37) was similar to using HLM $CL_{int,UGT}$ data obtained by substrate depletion. Use of metabolite formation $CL_{int,UGT}$ data obtained in the absence of BSA reduced the $f_{m,UGT}$ estimate. The $f_{m,UGT}$ determined in hepatocytes using the substrate depletion approach in the presence and absence of ABT (0.43) was similar to that determined from HLM. The in vitro $f_{m,UGT}$ for HKM and HIM were 1.0 due to the lack of CYP clearance observed in these tissues.

Prediction of propofol clearance and blood concentration-time profiles using data from different in vitro systems. Blood concentration-time profiles and in vivo clearance were predicted using various combinations of in vitro $CL_{int,UGT}$ and $CL_{int,CYP}$ data from the different systems used; a summary of the prediction accuracy for each system is shown in Table 3 (full details for individual dose groups are presented in Supplemental Data, Table 2). The predicted concentration-time profiles for all dose groups are shown in the Supplemental Data, Figures 4 and 5.

Use of the PBPK model resulted in under-estimation of clearance regardless of the source of the in vitro data. Predicted clearance did not exceed 35% of the observed values and recovery of the blood concentration-time profiles was poor when using CL_{int} data from all in vitro systems (Table 3). As expected from comparison of the in vitro data, no difference was observed in the predicted in vivo clearance from microsomal $CL_{int,UGT}$ data derived by either the substrate depletion or metabolite formation methods in the presence of BSA (Table 3). The lower in vitro CL_{int} obtained in hepatocytes or microsomes in the absence of BSA reduced the clearance prediction accuracy even further. Therefore, the microsomal CL_{int} data obtained using the substrate depletion approach (in the presence of BSA) were used for further analysis and optimization of the PBPK model; a representative predicted blood concentration-time profile obtained using these data is shown in

Downloaded from dmd.aspetjournals.org at ASPET Journals on April 18, 2024

DMD Fast Forward. Published on January 9, 2013 as DOI: 10.1124/dmd.112.050294
This article has not been copyedited and formatted. The final version may differ from this version.

Figure 3. When these in vitro data were used in the PBPK model, renal glucuronidation clearance contributed 11% of the predicted systemic clearance, which is much lower than the approximately 30% contribution that has been reported in vivo (Hiraoka et al., 2005; Takizawa et al., 2005a).

With microsomal substrate depletion clearance data as inputs, the PBPK model was used to predict the extraction ratio due to metabolic clearance for the kidney and the liver at steady state. These data were compared to corresponding in vivo values detailed in a clinical study (Hiraoka et al., 2005). Using in vitro data derived in the presence of BSA, an under-prediction of hepatic extraction was observed (predicted E_H was 0.39, which represented 42% of the observed value). A more pronounced under-prediction was found for E_R, with the predicted value (0.07) being only 10% of the observed value.

Optimization of the model for prediction of renal and hepatic metabolic clearance. Considering the under-prediction observed, in vitro clearance parameters were optimized within the PBPK model by performing simultaneous fitting of the concentration-time data from intact and anhepatic patients (Table 4); in vitro data from microsomal substrate depletion assays in the presence of BSA were used as the initial estimates of CL_{int}. Simultaneous optimization of in vitro hepatic and renal CL_{int} in the PBPK model showed that renal glucuronidation clearance was under-predicted to a greater extent than hepatic clearance, resulting in empirical scaling factor of 17 versus 9 required in the case of liver (Table 4). Coefficients of variation for the hepatic and renal CL_{int} empirical scaling factors were 59 and 39%, respectively (Table 4). Use of the empirical scaling factors solely for in vitro kidney $CL_{int,UGT}$ data, in conjunction with the 'non-optimized' liver $CL_{int,}$ resulted in predicted clearance within 2-fold (59% on average) of observed values. Representative blood concentration-time profiles predicted using either 'non-optimized' in vitro data or optimized renal and hepatic clearance (in vitro hepatic and renal CL_{int} data with the empirical scaling factors) are shown in Figure 3. A high degree of correlation was observed for this dataset (R^2 = 0.92, n = 94 data points) with 99% of the propofol blood concentrations predicted within 2-fold of the line of unity across the dose range (Figure 4). Use of the optimized in vitro clearance data in the PBPK model predicted an overall $f_{m,UGT}$ value of 0.53, in agreement with in vivo estimates of approximately 0.6 (Favetta et al., 2002). In addition, predicted E_H and E_R at steady state based on the use of the optimized scalars for in vitro hepatic and renal CL_{int} were within 20% of the observed values (91 and

Downloaded from dmd.aspetjournals.org at ASPET Journals on April 18, 2024

DMD Fast Forward. Published on January 9, 2013 as DOI: 10.1124/dmd.112.050294
This article has not been copyedited and formatted. The final version may differ from this version.

82% of observed values, respectively; data from an additional independent study (Hiraoka et al., 2005)).

Downloaded from dmd.aspetjournals.org at ASPET Journals on April 18, 2024

DMD Fast Forward. Published on January 9, 2013 as DOI: 10.1124/dmd.112.050294
This article has not been copyedited and formatted. The final version may differ from this version.

Discussion

This is the first study to assess the prediction accuracy of renal versus hepatic clearance from CL_{int} data determined in different in vitro systems by applying a PBPK modeling approach. Propofol was used as an example drug and clinical data reported in intact and anhepatic patients were utilized to refine the predictions of clearance from in vitro data and to optimize the PBPK model for prediction of propofol blood concentration-time profiles.

In vitro characterization of propofol metabolism in microsomes. No CYP clearance of propofol was detectable in HKM, in agreement with studies reporting low CYP mRNA levels in the kidney (Nishimura and Naito, 2006; Bieche et al., 2007). The effect of albumin on CYP2B6 (the main enzyme for propofol CYP metabolism) has not been investigated to date; this enzyme is not reported to be involved in free fatty acid clearance and a marked impact of albumin is not anticipated, in agreement with the minimal increase (2-fold) in $CL_{int,CYP}$ observed in HLM upon inclusion of BSA. Similar to previous reports, propofol liver $CL_{int,CYP}$ was greater than $CL_{int,UGT}$ (3-fold) in the absence of BSA with the extent of this difference being reduced upon inclusion of BSA (Al-Jahdari et al., 2006; Kilford et al., 2009).

The current study shows that the trend of increased $CL_{int,UGT}$ upon inclusion of albumin is consistent in hepatic, renal and intestinal microsomes; however, the extent differs between the tissues. Similarly to our findings, previous reports of the effect of albumin on UGT1A9 and 2B7 substrates in HLM also showed a decrease in K_m with minimal impact on V_{max} (Rowland et al., 2007; Rowland et al., 2008; Rowland et al., 2009). This is considered to be due to the sequestration of inhibitory free fatty acids released during microsomal incubations, allowing estimation of the true K_m (Rowland et al., 2007; Rowland et al., 2008). Propofol kinetic parameters obtained in HLM, HKM and HIM were comparable to previously published data, where available (Supplemental Data, Table 2). In the presence of BSA, HLM and HKM $CL_{int,UGT}$ values were similar from both metabolite formation and substrate depletion assays. In the current study, a decrease in the propofol V_{max} was observed at microsomal protein concentrations < 0.1 mg/ml and in the presence of BSA, in agreement with a previous report (Walsky et al., 2012). Similar effects were observed at both 1 and 2% BSA suggesting that the effect could not be simply rationalized by the differential concentration ratio of microsomal protein to BSA. Current findings are in contrast to an increase in V_{max} reported for other UGT1A9 substrates in the presence of BSA and at low microsomal protein concentrations (Manevski et al.,

Downloaded from dmd.aspetjournals.org at ASPET Journals on April 18, 2024

DMD Fast Forward. Published on January 9, 2013 as DOI: 10.1124/dmd.112.050294
This article has not been copyedited and formatted. The final version may differ from this version.

2011; Manevski et al., 2012). However, differences in assay conditions in the published studies prevent direct comparison to the findings herein; further investigation is required to confirm whether these effects on V_{max} are directly associated with the use of BSA at very low protein concentrations. Current findings highlight the importance of careful selection of the assay conditions when determining glucuronidation kinetic parameters in the presence of BSA, particularly when using microsomal protein concentrations of < 0.1 mg/mL.

The highest in vitro $f_{m,UGT}$ estimate was obtained from in house hepatocyte data (0.43), whereas the $f_{m,UGT}$ calculated from HLM in vitro data derived in the presence of BSA was < 0.4. These in vitro estimates ignore the contribution of extrahepatic metabolism and therefore it was not surprising that the fraction was lower than the value of 0.6 reported in vivo (Favetta et al., 2002). A mechanistic model that allows incorporation of metabolism in extrahepatic tissues is required to adequately assess the prediction of $f_{m,UGT}$ from in vitro CL_{int} data derived in both hepatic and extrahepatic microsomes. However, inclusion of such data in the PBPK model still resulted in an under-prediction of $f_{m,UGT}$ (0.39), with the predicted value being comparable to that derived from HLM data alone.

Prediction of propofol renal glucuronidation and hepatic metabolism using in vitro clearance data from different systems and optimization using in vivo data. The current study represents the first report where a PBPK model has been used to predict propofol renal metabolism from in vitro clearance data, in contrast to previous propofol PBPK modeling efforts that have mainly focused on accommodating potential lung sequestration (Levitt and Schnider, 2005; Upton and Ludbrook, 2005). Inclusion of BSA in the microsomal assays improved the prediction of propofol in vivo clearance using the PBPK model, consistent with the trend reported previously for UGT1A9 substrates using static IVIVE methods (Rowland et al., 2008; Kilford et al., 2009; Gill et al., 2012). However, the under-prediction trend was still apparent regardless of whether hepatocyte or microsomal data in the presence of 2% BSA were used as an input for hepatic CL_{int}; predicted clearance was < 35% of the observed value. Therefore, clinical data from three dose levels in intact patients and data reported for subjects during the anhepatic phase of liver transplantation were used to optimize the in vitro clearance parameters. Use of clinical data in conjunction with the developed PBPK model allowed differentiation between under-prediction of hepatic and renal CL_{int} and highlighted more pronounced under-estimation of propofol renal $CL_{int,UGT}$ in comparison to hepatic

Downloaded from dmd.aspetjournals.org at ASPET Journals on April 18, 2024

DMD Fast Forward. Published on January 9, 2013 as DOI: 10.1124/dmd.112.050294
This article has not been copyedited and formatted. The final version may differ from this version.

clearance (17- versus 9-fold). Prior to optimization, predicted extraction ratios were 0.07 and 0.42 for kidney and liver, compared to 0.43 - 0.87 and 0.76 - 0.98 estimated in vivo (Hiraoka et al., 2005; Takizawa et al., 2005a; Takizawa et al., 2005b). Following optimization of renal glucuronidation, the predicted in vivo clearance was within 2-fold of the observed values and the corresponding extraction ratios and $f_{m,UGT}$ values were in good agreement with the in vivo data (from independent studies than used for model development). The intestinal metabolism was not investigated in the PBPK model due to the anticipated low contribution of this tissue to its systemic clearance. This assumption is supported by UGT and CYP expression data for the intestine, showing low levels of UGT1A9 and CYP2B6 in comparison to the liver and kidney (Bieche et al., 2007; Harbourt et al., 2011; Court et al., 2012). Due to the lack of suitable in vivo data we could not assess the prediction accuracy for in vitro $CL_{int,UGT}$ data for the intestine or potential for propofol sequestration in either lungs or other tissues, although this cannot be ruled out.

Reported UGT mRNA data showed regional differences in the kidney (Gaganis et al., 2007; Lash et al., 2008). In addition, glucuronidation capacity has been found to differ between the sections of the kidney in laboratory animals, with the highest activity observed in the proximal tubular cells of the cortex (Cojocel et al., 1983; Hjelle et al., 1986). However, data on regional differences in glucuronidation activity in human kidney tissue are very limited. Two studies have shown up to 3-fold higher glucuronidation clearance for naproxen and morphine (mainly cleared by UGT2B7) in cortical compared to medullary microsomes (Yue et al., 1988; Gaganis et al., 2007). In contrast, frusemide (primarily cleared by UGT1A9) glucuronidation clearance was comparable in microsomes from human kidney cortex and medulla (Kerdpin et al., 2008). Although these data may suggest that there are no regional differences in glucuronidation clearance via UGT1A9 in the kidney, these findings should be considered with caution as potential differences in microsomal recovery depending on the region of the kidney were not considered. The information on the proportion of the cortex and medulla used for the preparation of the microsomes employed in the current study was not available; similarly, the region of the kidney used in the study reporting the kidney microsomal recovery (Al-Jahdari et al., 2006) is unknown, all of which may affect the glucuronidation activity and contribute to the particularly poor prediction of renal glucuronidation observed with the PBPK model prior to optimization of the in vitro data.

Downloaded from dmd.aspetjournals.org at ASPET Journals on April 18, 2024

DMD Fast Forward. Published on January 9, 2013 as DOI: 10.1124/dmd.112.050294
This article has not been copyedited and formatted. The final version may differ from this version.

Although we have successfully developed a PBPK model for the prediction of propofol clearance and exposure from in vitro CL_{int} data, we could not assess the use of our empirical scaling factors with other drugs. The availability of blood concentration-time data identifying drug metabolism across the kidney is extremely limited and hinders the assessment of this model with a wider range of compounds. In addition to the factors discussed above, poor prediction of renal metabolism may also suggest that well-stirred assumptions, which are adequate for many tissues in PBPK modeling, are not appropriate for the kidney and more complex models may need to be considered. This will be particularly relevant for drugs which are also substrates of the renal transporters (Giacomini et al., 2010). Unlike the liver, the kidney is not a homogeneous tissue and consists of distinct regions with varying blood flows. However, in vivo and in vitro data required for development and validation of more complex kidney models, such as absolute abundance data for the UGTs and transporters in the various regions of the kidney, are currently lacking in the literature.

In conclusion, the current study has shown consistent increases in propofol clearance estimates in hepatic, renal and intestinal microsomes due to the 'albumin effect' and highlighted the importance of careful selection of assay conditions when using BSA at very low microsomal protein concentrations. The analysis provides an example of the application of clinical data to refine the developed PBPK model and assess the predictive capacity of in vitro data for propofol renal and hepatic metabolic clearance in isolation. The current study highlighted a more pronounced under-prediction of renal glucuronidation than hepatic metabolism; further assessment of the contribution of extrahepatic clearance mechanisms and the adequacy of currently available scaling factors and models for renal metabolism are required.

Downloaded from dmd.aspetjournals.org at ASPET Journals on April 18, 2024

DMD Fast Forward. Published on January 9, 2013 as DOI: 10.1124/dmd.112.050294
This article has not been copyedited and formatted. The final version may differ from this version.

Acknowledgments

We thank Sue Murby and Dr. David Hallifax (University of Manchester) for valuable assistance with the LC-MS/MS, and Dr. Peter Kilford for determination of the hepatocyte in vitro clearance data.

Downloaded from dmd.aspetjournals.org at ASPET Journals on April 18, 2024

DMD Fast Forward. Published on January 9, 2013 as DOI: 10.1124/dmd.112.050294
This article has not been copyedited and formatted. The final version may differ from this version.

Authorship Contributions

Participated in research design: Gill, Gertz, Houston, and Galetin

Conducted Experiments: Gill

Contributed new reagents or analytical tools: N/A

Performed data analysis: Gill

Wrote or contributed to the writing of the manuscript: Gill, Gertz, Houston, and Galetin

Downloaded from dmd.aspetjournals.org at ASPET Journals on April 18, 2024

DMD Fast Forward. Published on January 9, 2013 as DOI: 10.1124/dmd.112.050294
This article has not been copyedited and formatted. The final version may differ from this version.

References

Al-Jahdari W, Yamamoto K, Hiraoka H, Nakamura K, Goto F, and Horiuchi R (2006) Prediction of total propofol clearance based on enzyme activities in microsomes from human kidney and liver. *Eur J Clin Pharmacol* **62:**527-533.

Barter ZE, Bayliss MK, Beaune PH, Boobis AR, Carlile DJ, Edwards RJ, Houston JB, Lake BG, Lipscomb JC, Pelkonen OR, Tucker GT, and Rostami-Hodjegan A (2007) Scaling factors for the extrapolation of in vivo metabolic drug clearance from in vitro data: Reaching a consensus on values of human microsomal protein and hepatocellularity per gram of liver. *Curr Drug Metab* **8:**33-45.

Bieche I, Narjoz C, Asselah T, Vacher S, Marcellin P, Lidereau R, Beaune P, and de Waziers I (2007) Reverse transcriptase-PCR quantification of mRNA levels from cytochrome (CYP)1, CYP2 and CYP3 families in 22 different human tissues. *Pharmacogenet Genomics* **17:**731-742.

Brown HS, Griffin M, and Houston JB (2007) Evaluation of cryopreserved human hepatocytes as an alternative in vitro system to microsomes for the prediction of metabolic clearance. *Drug Metab Dispos* **35:**293-301.

Brown RP, Delp MD, Lindstedt SL, Rhomberg LR, and Beliles RP (1997) Physiological parameter values for physiologically based pharmacokinetic models. *Toxicol Ind Health* **13:**407-484.

Cojocel C, Maita K, Pasino DA, Kuo C-H, and Hook JB (1983) Metabolic heterogeneity of the proximal and distal kidney tubules. *Life Sci* **33:**855-861.

Court MH (2005) Isoform-selective probe substrates for in vitro studies of human UDP-glucuronosyltransferases. *Methods Enzymol* **400:**104-116.

Court MH (2010) Interindividual variability in hepatic drug glucuronidation: Studies into the role of age, sex, enzyme inducers, and genetic polymorphism using the human liver bank as a model system. *Drug Metab Rev* **42:**209-224.

Court MH, Duan SX, Hesse LM, Venkatakrishnan K, and Greenblatt DJ (2001) Cytochrome P-450 2B6 is responsible for interindividual variability of propofol hydroxylation by human liver microsomes. *Anesthesiology* **94:**110-119.

Court MH, Zhang X, Ding X, Yee KK, Hesse LM, and Finel M (2012) Quantitative distribution of mRNAs encoding the 19 human UDP-glucuronosyltransferase enzymes in 26 adult and 3 fetal tissues. *Xenobiotica* **42:**266-277.

Downloaded from dmd.aspetjournals.org at ASPET Journals on April 18, 2024

DMD Fast Forward. Published on January 9, 2013 as DOI: 10.1124/dmd.112.050294
This article has not been copyedited and formatted. The final version may differ from this version.

Cubitt HE, Houston JB, and Galetin A (2009) Relative importance of intestinal and hepatic glucuronidation - impact on the prediction of drug clearance. *Pharm Res* **26:**1073-1083.

Cubitt HE, Houston JB, and Galetin A (2011) Prediction of human drug clearance by multiple metabolic pathways - integration of hepatic and intestinal microsomal and cytosolic data. *Drug Metab Dispos* **39:**864-873.

Dawidowicz AL, Fornal E, Mardarowicz M, and Fijalkowska A (2000) The role of human lungs in the biotransformation of propofol. *Anesthesiology* **93:**992-997.

Doenicke AW, Roizen MF, Rau J, O'Connor M, Kugler J, Klotz U, and Babl J (1997) Pharmacokinetics and pharmacodynamics of propofol in a new solvent. *Anesth Analg* **85:**1399-1403.

Favetta P, Degoute CS, Perdrix JP, Dufresne C, Boulieu R, and Guitton J (2002) Propofol metabolites in man following propofol induction and maintenance. *Br J Anaesth* **88:**653-658.

Fisher MB, Campanale K, Ackermann BL, VandenBranden M, and Wrighton SA (2000) In vitro glucuronidation using human liver microsomes and the pore-forming peptide alamethicin. *Drug Metab Dispos* **28:**560-566.

Fisher MB, Paine MF, Strelevitz TJ, and Wrighton SA (2001) The role of hepatic and extrahepatic UDP-glucuronosyltransferases in human drug metabolism. *Drug Metab Rev* **33:**273-297.

Gaganis P, Miners JO, Brennan JS, Thomas A, and Knights KM (2007) Human renal cortical and medullary UDP-glucuronosyltransferases (UGTs): Immunohistochemical localization of UGT2B7 and UGT1A enzymes and kinetic characterization of S-naproxen glucuronidation. *J Pharmacol Exp Ther* **323:**422-430.

Galetin A, Gertz M, and Houston JB (2008) Potential role of intestinal first-pass metabolism in the prediction of drug–drug interactions. *Expert Opin Drug Metab Toxicol* **4:**909-922.

Gepts EM, Camu FM, Cockshott IDP, and Douglas EJH (1987) Disposition of propofol administered as constant rate intravenous infusions in humans. *Anesth Analg* **66:**1256-1263.

Gertz M, Harrison A, Houston JB, and Galetin A (2010) Prediction of human intestinal first-pass metabolism of 25 CYP3A substrates from in vitro clearance and permeability data. *Drug Metab Dispos* **38:**1147-1158.

Downloaded from dmd.aspetjournals.org at ASPET Journals on April 18, 2024

DMD Fast Forward. Published on January 9, 2013 as DOI: 10.1124/dmd.112.050294
This article has not been copyedited and formatted. The final version may differ from this version.

Gertz M, Houston JB, and Galetin A (2011) Physiologically based pharmacokinetic modeling of intestinal first-pass metabolism of CYP3A substrates with high intestinal extraction. *Drug Metab Dispos* **39:**1633-1642.

Giacomini K, Huang S, Tweedie D, Benet L, Brouwer K, Chu X, Dahlin A, Evers R, Fischer V, Hillgren K, Hoffmaster K, Ishikawa T, Keppler D, Kim R, Lee C, Niemi M, Polli J, Sugiyama Y, Swaan P, Ware J, Wright S, Yee S, Zamek-Gliszczynski M, and Zhang L (2010) Membrane transporters in drug development. *Nat Rev Drug Discov* **9:**215-236.

Gill KL, Houston JB, and Galetin A (2012) Characterization of in vitro glucuronidation clearance of a range of drugs in human kidney microsomes: Comparison with liver and intestinal glucuronidation and impact of albumin. *Drug Metab Dispos* **40:**825-835.

Grounds RM, Twigley AJ, Carli F, Whitwam JG, and Morgan M (1985) The haemodynamic effects of intravenous induction. Comparison of the effects of thiopentone and propofol. *Anaesthesia* **40:**735-740.

Guitton J, Buronfosse T, Desage M, Flinois JP, Perdrix JP, Brazier JL, and Beaune P (1998) Possible involvement of multiple human cytochrome P450 isoforms in the liver metabolism of propofol. *Br J Anaesth* **80:**788-795.

Harbourt DE, Fallon JK, Ito S, Baba T, Ritter JK, Glish GL, and Smith PC (2011) Quantification of human uridine-diphosphate glucuronosyl transferase (UGT) 1A isoforms in liver, intestine and kidney using nano LC-MS/MS. *Anal Chem* **84:**98-105.

He Y-L, Ueyama H, Tashiro C, Mashimo T, and Yoshiya I (2000) Pulmonary Disposition of Propofol in Surgical Patients. *Anesthesiology* **93**.

Hiraoka H, Yamamoto K, Miyoshi S, Morita T, Nakamura K, Kadoi Y, Kunimoto F, and Horiuchi R (2005) Kidneys contribute to the extrahepatic clearance of propofol in humans, but not lungs and brain. *Br J Clin Pharmacol* **60:**176-182.

Hjelle JT, Hazelton GA, Klaassen CD, and Hjelle JJ (1986) Glucuronidation and sulfation in rabbit kidney. *J Pharmacol Exp Ther* **236:**150-156.

Huang SM and Rowland M (2012) The role of physiologically based pharmacokinetic modeling in regulatory review. *Clin Pharmacol Ther* **91:**542-549.

Downloaded from dmd.aspetjournals.org at ASPET Journals on April 18, 2024

DMD Fast Forward. Published on January 9, 2013 as DOI: 10.1124/dmd.112.050294
This article has not been copyedited and formatted. The final version may differ from this version.

ICRP (2002) *Publication 89 - Basic anatomical and physiological data for use in radiological protection: Reference values*. Pergamon for The International Commission on Radiological Protection.

Jones HM, Dickins M, Youdim K, Gosset JR, Attkins NJ, Hay TL, Gurrell IK, Logan YR, Bungay PJ, Jones BC, and Gardner IB (2011) Application of PBPK modelling in drug discovery and development at Pfizer. *Xenobiotica* **42:**94-106.

Kerdpin O, Knights KM, Elliot DJ, and Miners JO (2008) In vitro characterisation of human renal and hepatic frusemide glucuronidation and identification of the UDP-glucuronosyltransferase enzymes involved in this pathway. *Biochem Pharmacol* **76:**249-257.

Kilford PJ, Stringer R, Sohal B, Houston JB, and Galetin A (2009) Prediction of drug clearance by glucuronidation from in vitro data: Use of combined cytochrome P450 and UDP-glucuronosyltransferase cofactors in alamethicin-activated human liver microsomes. *Drug Metab Dispos* **37:**82-89.

Kirkpatrick T, Cockshott ID, Douglas EJ, and Nimmo WS (1988) Pharmacokinetics of propofol (Diprivan) in elderly patients. *Br J Anaesth* **60:**146-150.

Lash LH, Putt DA, and Cai H (2008) Drug metabolism enzyme expression and activity in primary cultures of human proximal tubular cells. *Toxicology* **244:**56-65.

Levitt D and Schnider T (2005) Human physiologically based pharmacokinetic model for propofol. *Anesthesiology* **5:**4.

Manevski N, Svaluto Morelo P, Yli-Kauhaluoma J, and Finel M (2011) Bovine serum albumin decreases the Km values of the human UDP-glucuronosyltransferases 1A9 and 2B7, but only in UGT1A9 it also largely increases the Vmax value. *Drug Metab Dispos* **39:**2117-2129.

Manevski NM, Yli-Kauhaluoma J, and Finel M (2012) UDP-glucuronic acid binds first and the aglycone substrate binds second to form a ternary complex in UGT1A9-catalyzed reactions, in both the presence and absence of BSA. *Drug Metab Dispos* **40:**2192-2203.

Mazoit JX, Sandouk P, Scherrmann JM, and Roche A (1990) Extrahepatic metabolism of morphine occurs in humans. *Clin Pharmacol Ther* **48:**613-618.

Nestorov I (2003) Whole Body Pharmacokinetic Models. *Clin Pharmacokinet* **42:**883-908.

Nestorov I (2007) Whole-body physiologically based pharmacokinetic models. *Expert Opin Drug Metab Toxicol* **3:**235-249.

Downloaded from dmd.aspetjournals.org at ASPET Journals on April 18, 2024

DMD Fast Forward. Published on January 9, 2013 as DOI: 10.1124/dmd.112.050294
This article has not been copyedited and formatted. The final version may differ from this version.

Nishimura M and Naito S (2006) Tissue-specific mRNA expression profiles of human phase I metabolizing enzymes except for cytochrome P450 and phase II metabolizing enzymes. *Drug Metab Pharmacokinet* **21:**357-374.

Oda Y, Hamaoka N, Hiroi T, Imaoka S, Hase I, Tanaka K, Funae Y, Ishizaki T, and Asada A (2001) Involvement of human liver cytochrome P4502B6 in the metabolism of propofol. *Br J Clin Pharmacol* **51:**281-285.

Pang K and Rowland M (1977) Hepatic clearance of drugs. I. Theoretical considerations of a "well-stirred" model and a "parallel tube" model. Influence of hepatic blood flow, plasma and blood cell binding, and the hepatocellular enzymatic activity on hepatic drug clearance. *J Pharmacokinet Biopharm* **5:**625-653.

Pichette V and du Souich P (1996) Role of the kidneys in the metabolism of furosemide: Its inhibition by probenecid. *J Am Soc Nephrol* **7:**345-349.

Poulin P, Jones RDO, Jones HM, Gibson CR, Rowland M, Chien JY, Ring BJ, Adkison KK, Ku MS, He H, Vuppugalla R, Marathe P, Fischer V, Dutta S, Sinha VK, Björnsson T, Lavé T, and Yates JWT (2011) PHRMA CPCDC initiative on predictive models of human pharmacokinetics, part 5: Prediction of plasma concentration–time profiles in human by using the physiologically-based pharmacokinetic modeling approach. *J Pharm Sci* **100:**4127-4157.

Price ML, Millar B, Grounds M, and Cashman J (1992) Changes in cardiac index and estimated systemic vascular resistance during induction of anaesthesia with thiopentone, methohexitone, propofol and etomidate. *Br J Anaesth* **69:**172-176.

Reiner GN, Labuckas DO, and García DA (2009) Lipophilicity of some GABAergic phenols and related compounds determined by HPLC and partition coefficients in different systems. *J Pharm Biomed Anal* **49:**686-691.

Rodgers T and Rowland M (2006) Physiologically based pharmacokinetic modelling 2: Predicting the tissue distribution of acids, very weak bases, neutrals and zwitterions. *J Pharm Sci* **95:**1238-1257.

Rowland A, Gaganis P, Elliot DJ, Mackenzie PI, Knights KM, and Miners JO (2007) Binding of inhibitory fatty acids is responsible for the enhancement of UDP-glucuronosyltransferase 2B7 activity by albumin: Implications for in vitro-in vivo extrapolation. *J Pharmacol Exp Ther* **321:**137-147.

Downloaded from dmd.aspetjournals.org at ASPET Journals on April 18, 2024

DMD Fast Forward. Published on January 9, 2013 as DOI: 10.1124/dmd.112.050294
This article has not been copyedited and formatted. The final version may differ from this version.

Rowland A, Knights KM, Mackenzie PI, and Miners JO (2008) The "albumin effect" and drug glucuronidation: Bovine serum albumin and fatty acid-free human serum albumin enhance the glucuronidation of UDP-glucuronosyltransferase (UGT) 1A9 substrates but not UGT1A1 and UGT1A6 activities. *Drug Metab Dispos* **36:**1056-1062.

Rowland A, Knights KM, Mackenzie PI, and Miners JO (2009) Characterization of the binding of drugs to human intestinal fatty acid binding protein (IFABP): Potential role of IFABP as an alternative to albumin for in vitro-in vivo extrapolation of drug kinetic parameters. *Drug Metab Dispos* **37:**1395-1403.

Rowland M, Peck C, and Tucker G (2011) Physiologically-based pharmacokinetics in drug development and regulatory science. *Annu Rev Pharmacol Toxicol* **51:**45-73.

Servin F, Cockshott ID, Farinotti R, Haberer JP, Winckler C, and Desmonts JM (1990) Pharmacokinetics of propofol infusions in patients with cirrhosis. *Br J Anaesth* **65:**177-183.

Servin F, Desmonts JM, Farinotti R, Haberer JP, and Wtnckler C (1988a) Pharmacokinetics of propofol administered by continuous infusion in patients with cirrhosis. *Anaesthesia* **43:**23-24.

Servin F, Desmonts JM, Haberer JP, Cockshott ID, Plummer GF, and Farinotti R (1988b) Pharmacokinetics and protein binding of propofol in patients with cirrhosis. *Anesthesiology* **69:**887-891.

Simons PJ, Cockshott ID, Douglas EJ, Gordon EA, Hopkins K, and Rowland M (1988) Disposition in male volunteers of a subanaesthetic intravenous dose of an oil in water emulsion of 14C-propofol. *Xenobiotica* **18:**429-440.

Soars MG, Burchell B, and Riley RJ (2002) In vitro analysis of human drug glucuronidation and prediction of in vivo metabolic clearance. *J Pharmacol Exp Ther* **301:**382-390.

Takizawa D, Hiraoka H, Goto F, Yamamoto K, and Horiuchi R (2005a) Human kidneys play an important role in the elimination of propofol. *Anesthesiology* **102:**327-330.

Takizawa D, Sato E, Hiraoka H, Tomioka A, Yamamoto K, Horiuchi R, and Goto F (2005b) Changes in apparent systemic clearance of propofol during transplantation of living related donor liver. *Br J Anaesth* **95:**643-647.

Upton RN and Ludbrook G (2005) A physiologically based, recirculatory model of the kinetics and dynamics of propofol in man. *Anesthesiology* **103:**344-352.

Downloaded from dmd.aspetjournals.org at ASPET Journals on April 18, 2024

DMD Fast Forward. Published on January 9, 2013 as DOI: 10.1124/dmd.112.050294
This article has not been copyedited and formatted. The final version may differ from this version.

Veroli P, O'Kelly B, Bertrand F, Trouvin JH, Farinotti R, and Ecoffey C (1992) Extrahepatic metabolism of propofol in man during the anhepatic phase of orthotopic liver transplantation. *Br J Anaesth* **68:**183-186.

Vree TB, Baars AM, and De Grood PMRM (1987) High-performance liquid chromatographic determination and preliminary pharmacokinetics of propofol and its metabolites in human plasma and urine. *J Chromatogr* **417:**458-464.

Walsky RL, Bauman JN, Bourcier K, Giddens G, Lapham K, Negahban A, Ryder TF, Obach RS, Hyland R, and Goosen TC (2012) Optimized assays for human UDP-glucuronosyltransferase (UGT) activities: Altered alamethicin concentration and utility to screen for UGT inhibitors. *Drug Metab Dispos* **40:**1051-1065.

Yue Q, Odar-Cederlöf I, Svensson J-O, and Säwe J (1988) Glucuronidation of morphine in human kidney microsomes. *Pharamcol Toxicol* **63:**337-341.

Zhao P, Zhang L, Grillo JA, Liu Q, Bullock JM, Moon YJ, Song P, Brar SS, Madabushi R, Wu TC, Booth BP, Rahman NA, Reynolds KS, Gil Berglund E, Lesko LJ, and Huang SM (2011) Applications of physiologically based pharmacokinetic (PBPK) modeling and simulation during regulatory review. *Clin Pharmacol Ther* **89:**259-267.

Downloaded from dmd.aspetjournals.org at ASPET Journals on April 18, 2024

DMD Fast Forward. Published on January 9, 2013 as DOI: 10.1124/dmd.112.050294
This article has not been copyedited and formatted. The final version may differ from this version.

Footnotes

The work was funded by a consortium of pharmaceutical companies within the Centre for Applied Pharmacokinetic Research at the University of Manchester and KLG is a recipient of a PhD studentship from Biotechnology and Biological Sciences Research Council, UK [Grant BB/F01760X/1].

Downloaded from dmd.aspetjournals.org at ASPET Journals on April 18, 2024

DMD Fast Forward. Published on January 9, 2013 as DOI: 10.1124/dmd.112.050294
This article has not been copyedited and formatted. The final version may differ from this version.

Legend to Figures

Figure 1: The structure of the whole body PBPK model used for prediction of propofol blood concentration-time profiles and clearance. Blood flow and tissue mass are presented for each compartment as a % of the whole body flow/mass for an average man. Remaining body mass and blood flow were accounted for in the 'rest of body' compartment. K_p values for each compartment were predicted using the Rodgers and Rowland method and normalised for observed V_{ss} ($V_{ss,obs}$) by a uniform scalar, scaling factor for volume = $V_{ss,obs}$ – blood volume / $V_{ss,pred}$ – blood volume. K_p for the 'rest of body' compartment was assumed to be the same as muscle.

Figure 2: Formation rate plots for propofol glucuronide as a function of substrate concentration in alamethicin activated human hepatic, renal and intestinal microsomes in the presence and absence of 2% BSA. Data represent the mean of three experiments, each performed in duplicate. Error bars represent the standard deviation. A: Data generated in the absence of BSA; B: Data generated in the presence of BSA. △, ○ and □ represent propofol glucuronide formation in hepatic, renal and intestinal microsomes, respectively.

Figure 3. Predicted blood concentration-time profiles for propofol using optimized liver and kidney in vitro $CL_{int,u}$ data derived from microsomes in the presence of BSA. ○ represent mean ± SD observed blood concentration-time data for the 18 mg/kg dose level from Gepts et al. (1987) (Gepts et al., 1987). Black line represents predicted concentrations using in vitro CL_{int} data from the substrate depletion microsomal assays (in the presence of BSA) without optimization; red line represents predicted concentrations using optimized kidney $CL_{int,UGT}$ data; green line represents predicted concentrations using optimized CL_{int} data for both liver and kidney.

Figure 4: Comparison of observed and predicted propofol blood concentrations using the whole body PBPK model to simultaneously optimize liver and kidney CL_{int}. Solid line represents unity; dashed line represents a 2-fold deviation from unity; ○ represents data from anhepatic patients (Veroli et al., 1992); x, ◇ and □ represent data from the 6, 12 and 18 mg/kg dose levels in intact patients (Gepts et al., 1987), respectively.

Downloaded from dmd.aspetjournals.org at ASPET Journals on April 18, 2024

TABLE 1

Study details for clinical data used during validation and optimization of a whole body PBPK model for prediction of propofol in vivo clearance and blood concentration-time profiles from in vitro CL_{int} data

Study	Status of patients	Dose type	Dose level (mg/kg)	Number of subjects	Mean body weight (± SD) (kg)	Mean Age (± SD) (Years)	% Male
(Doenicke et al., 1997)	Intact	Intravenous bolus	2	12	ND	24 – 42 [a]	100
			2	12	ND	24 – 42 [a]	100
(Gepts et al., 1987)	Intact	Intravenous Infusion over 2 h	6	6	75.0 (7.2)	60.3 (4.9)	100
			12	6	65.5 (7.9)	50.6 (14.7)	67
			18	6	61.6 (8.8)	39.8 (10.0)	50
(Veroli et al., 1992)	Anhepatic	Intravenous Bolus	0.5	10	60.0 (7.0)	38.0 (ND)	ND

ND = Not detailed

[a] mean age not detailed, age range of subjects presented instead

Downloaded from dmd.aspetjournals.org at ASPET Journals on April 18, 2024

DMD Fast Forward. Published on January 9, 2013 as DOI: 10.1124/dmd.112.050294
This article has not been copyedited and formatted. The final version may differ from this version.

TABLE 2

Kinetic parameters from different in vitro assays used to characterize propofol $CL_{int,CYP}$ and $CL_{int,UGT}$ in the presence and absence of 2% BSA and used in a whole body PBPK model to predict propofol in vivo clearance and blood concentration-time profiles

Assay Type	Parameter	Without BSA				With 2% BSA		
		HLM	HKM	HIM	Hepatocytes	HLM	HKM	HIM
Metabolite Formation	V_{max} (pmol/min/mg protein)	1460 (244)	5220 (726)	1280 (147)	NT	1390 (101)	4310 (1406)	1470 (457)
	K_m (μM)	107 (39.9)	91.0 (12.8)	458 (65.4)	NT	5.22 (0.360)	3.45 (0.931)	133 (55.6)
	$CL_{int,UGT}$ (mL/min/g tissue) [a]	0.594 (0.215)	0.735 (0.0247)	0.0581 (0.00652)	NT	10.6 (0.936)	17.0 (7.62)	0.237 (0.0551)
Substrate Depletion	$CL_{int,UGT}$ (mL/min/g tissue) [a, b]	2.71 (0.18)	1.17 (0.41)	1.29 (-)	7.63 [c] (1.68)	8.05 (0.46)	13.1 (1.66)	2.13 (-)
	$CL_{int,CYP}$ (mL/min/g tissue) [a]	9.12 (2.03)	ND	ND	10.2 [d]	18.1 (0.455)	ND	ND
	$CL_{int,CYP \& UGT}$ (mL/min/g tissue) [a]	NT	NT	NT	17.9 [c] (3.36)	NT	NT	NT

Data are the mean (SD) of n = 3 experiments, each performed in duplicate, with the exception of $CL_{int,UGT}$ in HIM substrate depletion assays where n = 1.

NA = not applicable; ND = no depletion observed; NT = not tested.

Downloaded from dmd.aspetjournals.org at ASPET Journals on April 18, 2024

DMD Fast Forward. Published on January 9, 2013 as DOI: 10.1124/dmd.112.050294
This article has not been copyedited and formatted. The final version may differ from this version.

[a] In vitro CL_{int} data scaled with microsomal recovery factors (40, 12.8 and 20.6 mg protein/g tissue for HLM, HKM and HIM, respectively) or hepatocellularity (120×10^6 cells/g tissue) to give scaled CL_{int} per gram of tissue.

[b] Data presented previously in Gill et al. (2012) (Gill et al., 2012).

[c] In house data; where $CL_{int,CYP}$ and $_{UGT}$ was determined in hepatocytes in the absence of ABT and $CL_{int,UGT}$ was determined in hepatocytes in the presence of ABT.

[d] Hepatocyte CL_{int} in absence of ABT – hepatocyte CL_{int} in presence of ABT.

DMD Fast Forward. Published on January 9, 2013 as DOI: 10.1124/dmd.112.050294
This article has not been copyedited and formatted. The final version may differ from this version.

Downloaded from dmd.aspetjournals.org at ASPET Journals on April 18, 2024

TABLE 3

Accuracy of propofol in vivo clearance predicted using $CL_{int,CYP}$ and $CL_{int,UGT}$ data derived from different in vitro systems

In vitro method used to obtain microsomal $CL_{int,UGT}$	Mean (SD) Predicted CL / Observed CL (%)		
	In vitro systems used		
	Microsomes without BSA	Microsomes with BSA	Hepatocytes and HKM & HIM with BSA
Substrate depletion	16.8 (2.19)	33.1 (4.78)	28.3 (3.54)
Metabolite formation	13.7 (1.75)	34.7 (5.15)	26.4 (3.59) [a]

Data for individual dose groups detailed in Supplemental Data, Table 2.

[a] Substrate depletion approach used to determine hepatocyte CL_{int} data.

Downloaded from dmd.aspetjournals.org at ASPET Journals on April 18, 2024

DMD Fast Forward. Published on January 9, 2013 as DOI: 10.1124/dmd.112.050294
This article has not been copyedited and formatted. The final version may differ from this version.

TABLE 4

Empirical scaling factors use for prediction of K_p values and in vitro hepatic and renal CL_{int} data determined by optimization of the PBPK model using simultaneous fitting of in vivo concentration-time data from intact and anhepatic patients

Parameter	Initial parameter estimate	Model fitted parameter estimate [a]	Model fitted scalar [a]	CV% for fitted scalar [a]
K_p [b]	-	-	0.54	9.5
Renal $CL_{int,UGT}$ (l/h/g tissue)	0.786 [c]	13.6	17.3	39
Hepatic CL_{int} [d] (l/h/g tissue)	1.57 [c]	14.5	9.21	59

CV = coefficient of variation.

[a] Parameters estimated by simultaneous fitting of in vivo concentration-time data from intact and anhepatic patients, as detailed in the methods section.

[b] Initial K_p values estimated using the Rodgers and Rowland method (Rodgers and Rowland, 2006).

[c] Initial CL_{int} data taken from microsomal substrate depletion assays in the presence of BSA, full details presented in Table 2.

[d] Combined $CL_{int,CYP}$ and $CL_{int,UGT}$ data.

Downloaded from dmd.aspetjournals.org at ASPET Journals on April 18, 2024

DMD Fast Forward. Published on January 9, 2013 as DOI: 10.1124/dmd.112.050294
This article has not been copyedited and formatted. The final version may differ from this version.

Figure 1

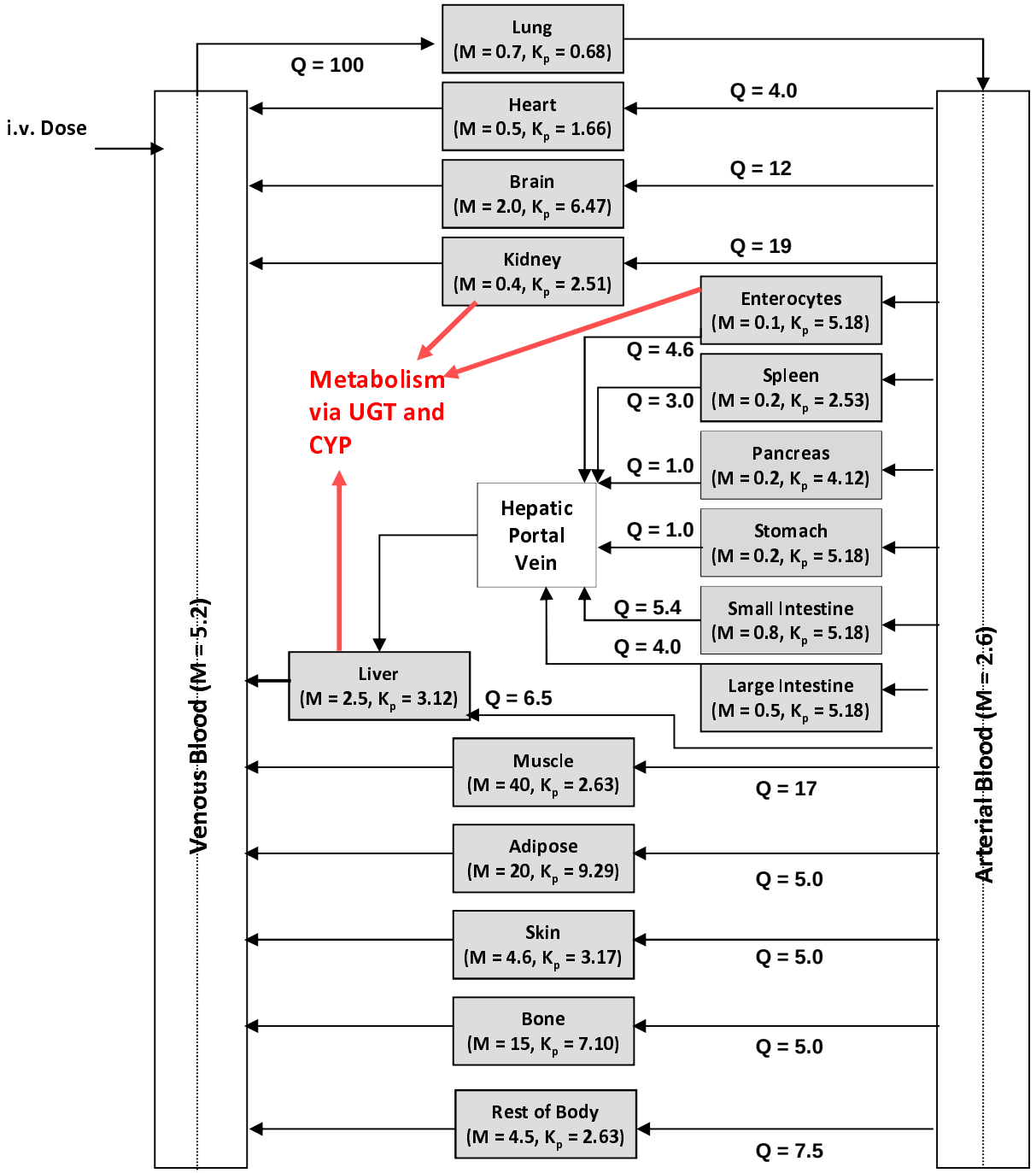

Downloaded from dmd.aspetjournals.org at ASPET Journals on April 18, 2024

DMD Fast Forward. Published on January 9, 2013 as DOI: 10.1124/dmd.112.050294
This article has not been copyedited and formatted. The final version may differ from this version.

Figure 2

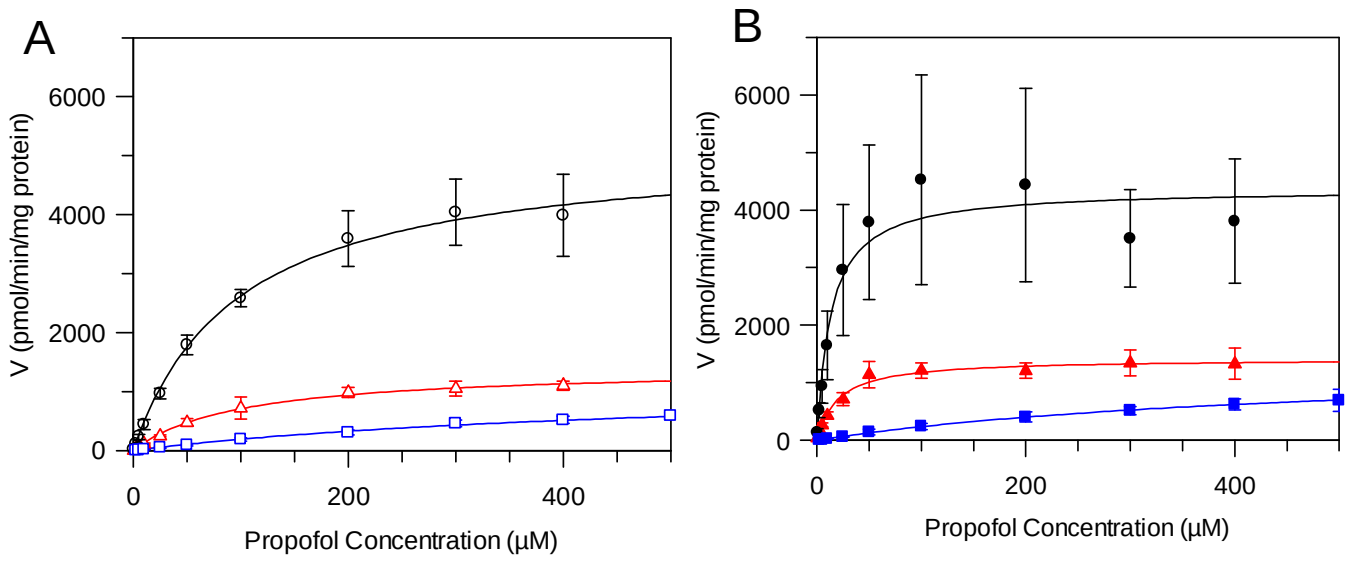

DMD Fast Forward. Published on January 9, 2013 as DOI: 10.1124/dmd.112.050294
This article has not been copyedited and formatted. The final version may differ from this version.

Downloaded from dmd.aspetjournals.org at ASPET Journals on April 18, 2024

Figure 3

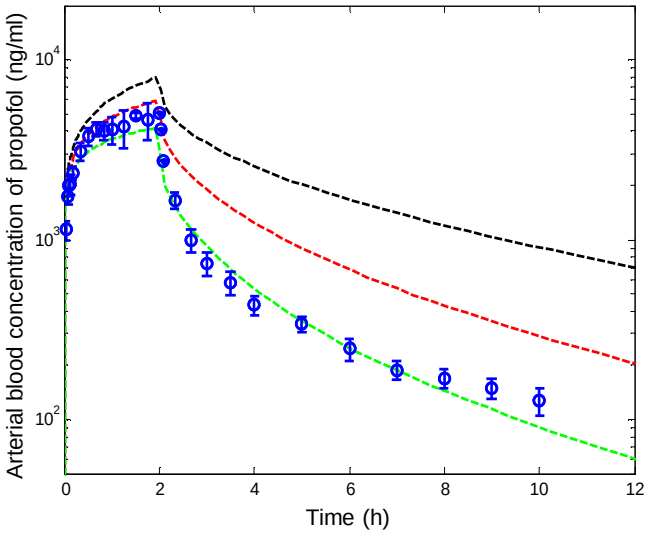

DMD Fast Forward. Published on January 9, 2013 as DOI: 10.1124/dmd.112.050294
This article has not been copyedited and formatted. The final version may differ from this version.

Downloaded from dmd.aspetjournals.org at ASPET Journals on April 18, 2024

Figure 4

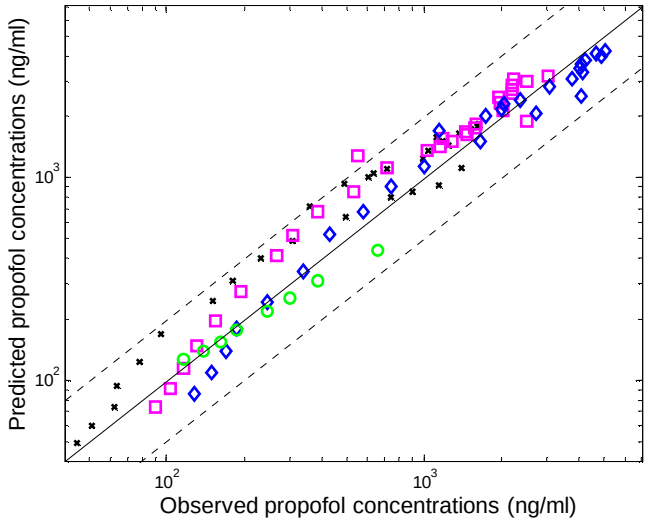

DMD Fast Forward. Published on January 9, 2013 as DOI: 10.1124/dmd.112.050294
This article has not been copyedited and formatted. The final version may differ from this version.

Downloaded from dmd.aspetjournals.org at ASPET Journals on April 18, 2024